

A new test for the Galactic formation and evolution – prediction for the orbital eccentricity distribution of the halo stars

K. Hattori* and Y. Yoshii*

Institute of Astronomy, School of Science, University of Tokyo, Tokyo 181-0015, Japan

Accepted 2010 May 11. Received 2010 May 10; in original form 2009 December 10

ABSTRACT

We present theoretical calculations for the differential distribution of stellar orbital eccentricity in a galaxy halo, assuming that the stars constitute a spherical, collisionless system in dynamical equilibrium with a dark matter halo. In order to define the eccentricity e of a halo star for given energy E and angular momentum L , we adopt two types of gravitational potential, such as an isochrone potential and a Navarro-Frenk-White potential, that could form two ends covering in-between any realistic potential of dark matter halo. Based on a distribution function of the form $f(E, L)$ that allows constant anisotropy in velocity dispersions characterized by a parameter β , we find that the eccentricity distribution is a monotonically increasing function of e for the case of highly radially anisotropic velocity dispersions ($\beta \gtrsim 0.6$), while showing a hump-like shape for the cases from radial through tangential velocity anisotropy ($\beta \lesssim 0.6$). We also find that when the velocity anisotropy agrees with that observed for the Milky Way halo stars ($\beta \simeq 0.5 - 0.7$), a nearly linear eccentricity distribution of $N(e) \propto e$ results at $e \lesssim 0.7$, largely independent of the potential adopted. Our theoretical eccentricity distribution would be a vital tool of examining how far out in the halo the dynamical equilibrium has been achieved, through comparison with kinematics of halo stars sampled at greater distances. Given that large surveys of the SEGUE and Gaia projects would be in progress, we discuss how our results would serve as a new guide in exploring the formation and evolution of the Milky Way halo.

Key words: Galaxy: halo – Galaxy: kinematics and dynamics – Galaxy: formation – Galaxy: evolution – stellar dynamics – methods: analytical.

1 INTRODUCTION

Studies of large-scale structures in the universe and fluctuations in the cosmic microwave background strongly favor a Λ -cold dark matter (Λ CDM) cosmology (e.g., Cole et al. 2005; Dunkley et al. 2009). The formation of structures in this cosmology is a process of hierarchical clustering, in the sense that numerous CDM lumps cluster gravitationally and merge together to form larger structures (White & Rees 1978; Blumenthal et al. 1984).

Dark halos of galaxy systems are similarly formed via clustering of subhalos as a result of CDM agglomerations that reach the maximum expansion then turn around to collapse in the background expanding medium, but a detailed process leading to the halo formation from primordial density fluctuations is highly nonlinear and is not as simple as

the formation of larger structures in the universe (e.g., for review see Ostriker 1993 and Bertschinger 1998).

High-resolution Λ CDM simulations for the halo formation generically show that mergers and collisions of subhalos induce the overall collapse and virialize the inner region of host halo, while surviving subhalos orbit as separate entities within the inner virialized region of halo (e.g., Moore et al. 1999; Ghigna et al. 2000; Helmi, White & Springel 2003; Valluri et al. 2007). A majority of stars formed through this build-up of halo are expected to have also experienced the redistribution of energy and momentum that drives the phase mixing or violent relaxation towards the dynamical equilibrium (Lynden-Bell 1967). This leads to an idea that a stellar halo, which can be regarded as a collisionless system, holds the dynamical information just after the last violent relaxation in forming the halo.

We then take an approach to find out the relics of the formation of the Milky Way halo from the kinematics of halo stars. Among many of their kinematic properties available at

* E-mail: khattori@ioa.s.u-tokyo.ac.jp (KH); yoshii@ioa.s.u-tokyo.ac.jp (YY)

present and in the near future, the differential distribution of stellar orbital eccentricity $N(e)$ seems to be of special importance. The orbital eccentricity of a star is a quasi-adiabatic invariant (Eggen, Lynden-Bell & Sandage 1962; Lynden-Bell 1963) and is unaffected by the small and slow variation of the gravitational potential that might have occurred after the major formation of halo stars. It is therefore most likely that the shape of $N(e)$ has been conserved until present. With this consideration, comparing the observed shape of $N(e)$ for halo stars with the theoretical one for the halo in dynamical equilibrium, we could explore how far out in the halo the dynamical equilibrium was achieved. Consequently, $N(e)$ serves as a new test of halo formation scenario in a Λ CDM cosmology.

As a useful way to derive $N(e)$ theoretically, we consider the orbit of halo stars in assumed gravitational potentials of the halo. In section 2, we present our formulation to calculate $N(e)$ under some plausible assumptions for the halo, and apply it to two extreme gravitational potentials of academic interest. The results for realistic cases are shown for the isochrone potential and for the Navarro-Frenk-White (NFW) potential in section 3. We summarize the results and discuss the prospects of investigating the formation and evolution of the Milky Way halo in section 4.

2 FORMULATION

We assume that the halo stars constitute a spherical, collisionless system in dynamical equilibrium with a dark halo. Since the dark matter is known to dominate the total mass of the galaxy system, the motion of halo stars is governed by the gravitational potential of dark halo.

2.1 Stellar orbital eccentricity in a model halo

When a spherical halo potential $V(r)$ is given with respect to the galaxy center, the energy E and the angular momentum L of a star at the position \mathbf{r} with the velocity \mathbf{v} are written respectively as

$$E = \frac{1}{2}\mathbf{v}^2 + V(r), \quad \text{and} \quad L = |\mathbf{L}| = |\mathbf{r} \times \mathbf{v}|, \quad (1)$$

where $r = |\mathbf{r}|$. The orbital eccentricity of a star is practically defined as

$$e \equiv \frac{r_{\text{apo}} - r_{\text{peri}}}{r_{\text{apo}} + r_{\text{peri}}}, \quad (2)$$

where r_{apo} and r_{peri} are the apo- and peri-centric distances, respectively, and are given by two real solutions ($r_{\text{apo}} > r_{\text{peri}}$) of the following equation:

$$E = V(r) + \frac{L^2}{2r^2} \equiv V_{\text{eff}}(L; r). \quad (3)$$

It is evident from equations (2) and (3) that a pair of (E, L) has a one-to-one correspondence to (E, e) , but there is a region of (E, L) in which two real solutions are not allowed and thus, except for the case of circular orbits, the eccentricity cannot be defined. Since such unbound orbits do not form a steady population of stellar halo, we neglect them and exclusively consider stars with bound orbits. Constraints on E and L that allow bound orbits are presented in Appendix A.

2.2 Differential distribution of stellar orbital eccentricity

Let $f(\mathbf{r}, \mathbf{v})$ be the distribution function of halo stars, then the number of halo stars in a phase space volume $d^3\mathbf{r}d^3\mathbf{v}$ centered at (\mathbf{r}, \mathbf{v}) is given by $f(\mathbf{r}, \mathbf{v})d^3\mathbf{r}d^3\mathbf{v}$. According to the strong Jeans theorem, the distribution function should be expressed in terms of isolating integrals only (Lynden-Bell 1960, 1962). For a spherical system that is invariant under rotation, it takes a form of either $f(E)$ or $f(E, L)$, depending on whether the stellar velocity dispersion is isotropic or anisotropic, respectively.

The velocity dispersion observed for halo stars is radially anisotropic (e.g., Yoshii & Saio 1979; Gilmore, Wyse, & Kuijken 1989). Furthermore, recent observations for halo stars within the distance of 10 kpc away from us show that the shape of velocity ellipsoid is constant and its principal axes are well aligned with the spherical coordinates (Carollo et al. 2007; Bond et al. 2009). If we extrapolate this fact to a whole system, one simple form of the distribution function is

$$f(E, L) = \begin{cases} g(E)L^{-2\beta}, & \text{if } (E, L) \text{ is 'allowed'} \\ 0, & \text{otherwise,} \end{cases} \quad (4)$$

where $g(E)$ is a function of E (e.g., Binney & Tremine 2008). Here, β is a constant value of velocity anisotropy parameter defined as

$$\beta \equiv 1 - \frac{\sigma_t^2}{\sigma_r^2}, \quad (5)$$

where σ_r is the radial velocity dispersion and σ_t is the tangential velocity dispersion projected onto the spherical $\theta - \phi$ surface. Although β is about 0.5 – 0.7 observationally (e.g., Bond et al. 2009; Smith et al. 2009; Carollo et al. 2010), we will use it as a constant parameter below.

By changing the variables and integrating over the spherical coordinates, the number of stars in $d^3\mathbf{r}d^3\mathbf{v}$ reduces to

$$N(E, L)dEdL^2 = 4\pi^2 g(E)L^{-2\beta} T_r dEdL^2, \quad (6)$$

with the radial period of stellar orbit given by

$$T_r(E, L) \equiv \oint \frac{dr}{v_r} = 2 \int_{r_{\text{peri}}}^{r_{\text{apo}}} \frac{dr}{\sqrt{2[E - V_{\text{eff}}(L; r)]}}. \quad (7)$$

Since L^2 is a function of E and e , we here introduce the E -dependent differential eccentricity distribution as

$$n_\beta(E, e) = 4\pi^2 L^{-2\beta} \cdot T_r \cdot \left| \left(\frac{\partial L^2}{\partial e} \right)_E \right|. \quad (8)$$

We then express the differential eccentricity distribution as

$$N_\beta(e) = \int_{\text{allowed } E} g(E) n_\beta(E, e) dE. \quad (9)$$

It is apparent from this equation that $N_\beta(e)$ is a weighted sum of $n_\beta(E, e)$ with a weight function of $g(E)$. Thus, once the gravitational potential $V(r)$ and the velocity anisotropy parameter β are specified, we can formally obtain $n_\beta(E, e)$, and also $N_\beta(e)$ after integrating $n_\beta(E, e)$ over E with its appropriate weight.

2.3 Extreme cases of mass distribution

In this subsection, mostly for pedagogical purpose, we consider two extreme cases of mass distribution such as the point mass at the center and the homogeneous distribution in the truncated sphere. These cases allow analytic expression of $n_\beta(E, e)$, and because it is separable in E and e , $N_\beta(e)$ can also be obtained except for its normalization. Therefore, these cases are helpful to understand the results for any more realistic cases.

2.3.1 Central point mass

The gravitational potential arising from the central point mass is Keplerian and is given by

$$V(r) = -\frac{GM}{r}, \quad (10)$$

where M is the total mass of dark halo and G is the gravitational constant. For bound orbits with $E < 0$, there are two real and positive solutions for equation (3), or equivalently,

$$(-2E)r^2 - 2GMr + L^2 = 0. \quad (11)$$

The orbital eccentricity is expressed in terms of (E, L) as

$$e = \sqrt{1 - \frac{(-2E)L^2}{(GM)^2}}, \quad (12)$$

and the other relevant quantities are neatly expressed as

$$T_r = \frac{2\pi GM}{(-2E)^{\frac{3}{2}}}, \quad \text{and} \quad L^2 = \frac{(GM)^2}{-2E}(1 - e^2). \quad (13)$$

Substitution of these quantities in equations (8) and (9) gives the E -dependent differential eccentricity distribution

$$n_\beta(E, e) = 16\pi^3 (GM)^{3-2\beta} (-2E)^{\beta-\frac{5}{2}} \frac{e}{(1-e^2)^\beta}, \quad (14)$$

and the differential eccentricity distribution

$$N_\beta(e) = 16\pi^3 (GM)^{3-2\beta} \left[\int g(E) (-2E)^{\beta-\frac{5}{2}} dE \right] \frac{e}{(1-e^2)^\beta}. \quad (15)$$

Since $N_\beta(e) \propto n_\beta(E, e)$, we normalize $N_\beta(e)$ such that $\int_0^1 N_\beta(e) de = 1$, and write

$$\text{normalized } N_\beta(e) = 2(1-\beta) \frac{e}{(1-e^2)^\beta}, \quad (\beta \neq 1). \quad (16)$$

The results of $N_\beta(e)$ for several values of β are shown on the left panel of Figure 1. For the case of $\beta = 0$ (isotropic velocity dispersion), $N_\beta(e)$ is exactly proportional to e (Binney & Tremaine 2008) and we call it the linear eccentricity distribution. For $0 < \beta < 1$ (radially anisotropic velocity dispersion), $N_\beta(e)$ is a rapidly increasing function of e with a peak always at $e = 1$. On the other hand, for $\beta < 0$ (tangentially anisotropic velocity dispersion), $N_\beta(e)$ shows a hump-like e -distribution around a single peak at $e = (1 - 2\beta)^{-1/2}$.

We should notice that the linear trend of $N_\beta \propto e$ prevails in a range of $0 < e < 0.3$ regardless of β , while the behavior of $N_\beta(e)$ is very sensitive to β in a range of $0.6 < e < 1$ and the difference there clearly shows up.

2.3.2 Truncated homogeneous sphere

A homogeneous density distribution within truncated sphere is expressed as

$$\rho(r) = \begin{cases} \frac{3M}{4\pi r_t^3}, & \text{if } r < r_t \\ 0, & \text{otherwise,} \end{cases} \quad (17)$$

where M is the total mass of dark halo and r_t is the truncation radius. The gravitational potential arising from this density distribution is given by

$$V(r) = \begin{cases} -\frac{3GM}{2r_t} + \frac{GM}{2r_t} \left(\frac{r}{r_t}\right)^2, & \text{if } r < r_t \\ -\frac{GM}{r}, & \text{otherwise.} \end{cases} \quad (18)$$

We consider only stars with $E < E_t \equiv -GM/r_t$, which guarantees the stars to be confined inside the truncated radius r_t . Thus, bound orbits within the truncated sphere are allowed if $E_{\min} < E < E_t$ where we note $E_{\min} \equiv (3/2)E_t$. In this limited range of E , there are two real and positive solutions for equation (3), or equivalently,

$$GM r_t \left(\frac{r}{r_t}\right)^4 - 2(E - E_{\min}) r_t^2 \left(\frac{r}{r_t}\right)^2 + L^2 = 0, \quad (19)$$

if and only if

$$0 < D < 1, \quad (20)$$

where

$$D = \frac{GML^2}{r_t^3(E - E_{\min})^2}. \quad (21)$$

The orbital eccentricity is expressed in terms of D as

$$e = \sqrt{\frac{1 - \sqrt{D}}{1 + \sqrt{D}}}, \quad (22)$$

and the other relevant quantities are expressed in terms of (E, L) as

$$T_r = \pi \sqrt{\frac{r_t^3}{GM}}, \quad \text{and} \quad L^2 = \frac{r_t^3}{GM} (E - E_{\min})^2 \left(\frac{1 - e^2}{1 + e^2}\right)^2. \quad (23)$$

Consequently, we obtain

$$n_\beta(E, e) = 32\pi^3 \left(\frac{r_t^3}{GM}\right)^{\frac{3}{2}-\beta} (E - E_{\min})^{2-2\beta} \frac{e(1-e^2)^{1-2\beta}}{(1+e^2)^{3-2\beta}}, \quad (24)$$

and

$$N_\beta(e) = 32\pi^3 \left(\frac{r_t^3}{GM}\right)^{\frac{3}{2}-\beta} \left[\int g(E) (E - E_{\min})^{2-2\beta} dE \right] \times \frac{e(1-e^2)^{1-2\beta}}{(1+e^2)^{3-2\beta}}. \quad (25)$$

As in the point mass model, since $N_\beta(e) \propto n_\beta(E, e)$, we normalize $N_\beta(e)$ such that $\int_0^1 N_\beta(e) de = 1$, and write

$$\text{normalized } N_\beta(e) = 8(1-\beta) \frac{e(1-e^2)^{1-2\beta}}{(1+e^2)^{3-2\beta}}, \quad (\beta \neq 1). \quad (26)$$

The results of $N_\beta(e)$ for several values of β are shown

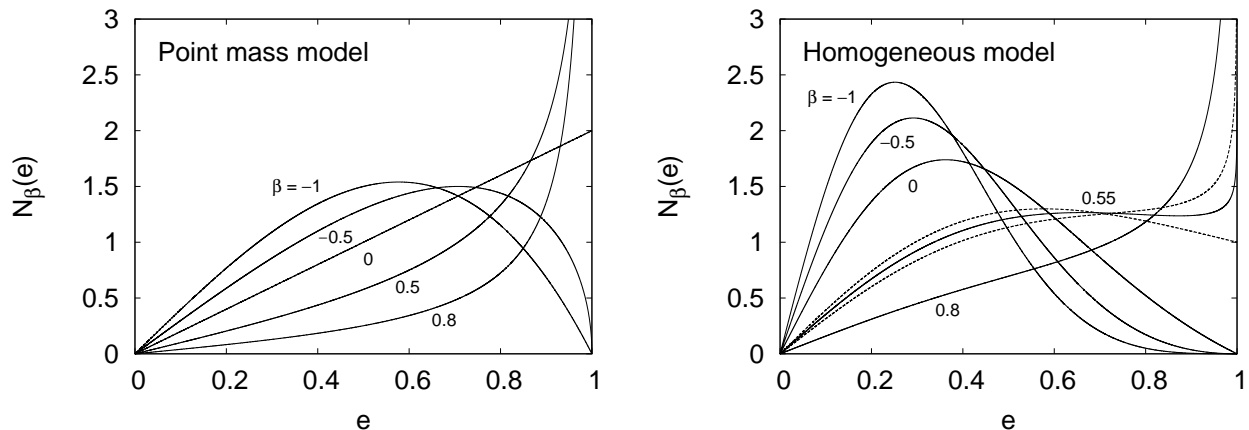


Figure 1. Differential distribution of stellar orbital eccentricity $N_\beta(e)$ in two extreme cases of mass distribution, such as the point mass model on the left panel and the homogeneous model on the right panel. The results are shown by lines for several values of velocity anisotropy parameter β . If $N_\beta(e)$ near $e = 1$ sensitively changes at some particular value of β , the results for $\beta \pm 0.05$ are additionally shown by dotted lines for the purpose of illustrating its sensitivity. Note that $N_\beta(e)$ is normalized such that $\int_0^1 N_\beta(e) de = 1$.

on the right panel of Figure 1. For $\beta < 0.5$, $N_\beta(e)$ shows a hump-like e -distribution with a single peak at

$$e_{\text{peak}} = \sqrt{\frac{4(1-\beta) - \sqrt{13 - 32\beta + 16\beta^2}}{3}}. \quad (27)$$

For $0.5 < \beta < 1 - \sqrt{3}/4$, however, $N_\beta(e)$ has two local maxima such as a broad peak at $e = e_{\text{peak}}$ and a sharp peak at $e = 1$. Overall behavior monotonically increases with e in a range of $0 < e < e_{\text{peak}}$, and is kept more or less flat in the range of $e_{\text{peak}} < e < 1$. For $1 - \sqrt{3}/4 < \beta < 1$, $N_\beta(e)$ is a rapidly increasing function of e .

For a given value of β , $N_\beta(e)$ is more weighted at smaller e in the homogeneous model, when compared with the point mass model. In particular, for $\beta = 0$ (isotropic velocity dispersion), $N_\beta(e)$ shows a broad hump-like e -distribution around a peak at $e_{\text{peak}} = 0.36$ in the homogeneous model, while showing an exactly linear e -distribution in the point mass model. This sensitivity, though between two extreme cases, could be used to discriminate the likely mass distribution in more realistic cases to be considered in section 3.

2.4 Effect of central mass concentration

In the cases of central point mass and truncated homogeneous sphere, the shape of $n_\beta(E, e)$ is the same as $N_\beta(e)$, because $n_\beta(E, e)$ is separable in E and e and thus the shape of $N_\beta(e)$ is unaffected by $g(E)$ in equation (4). This property generally holds when the density distribution in the truncated sphere is given by $\rho(r) \propto 1/r^\gamma$ (see Appendix B). The homogeneous model in section 2.3.2 corresponds to $\gamma = 0$.

Using the cases of $\gamma = 1$ (linear potential model) and $\gamma = 2$ (singular isothermal model) that are intermediate between two extreme cases considered above, we can examine how $N_\beta(e)$ depends on the central mass concentration. As shown in Figure 2 for $\beta = 0$, there is a clear trend that the e -distribution is peaked at larger e as the halo mass is more centrally concentrated. This trend is also true regardless of

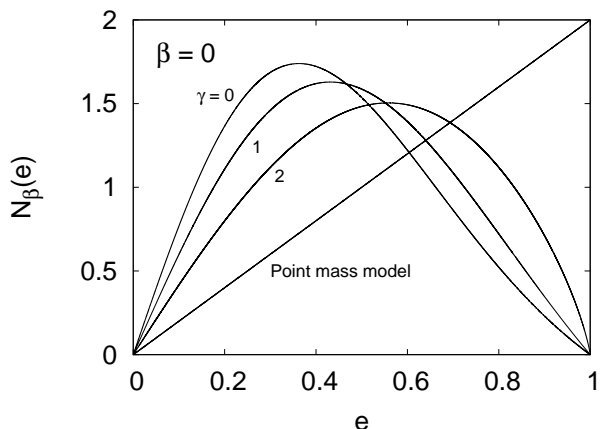


Figure 2. Differential distribution of stellar orbital eccentricity $N_\beta(e)$ for four types of model potentials, when the stellar velocity dispersion is isotropic ($\beta = 0$). Considered are the homogeneous model ($\gamma = 0$, section 2.3.2), the linear potential model ($\gamma = 1$, Appendix B.1), the singular isothermal model ($\gamma = 2$, Appendix B.2), and the point mass model (section 2.3.1), in order of increasing the central mass concentration. There is a clear trend that the e -distribution is peaked at larger e as the halo mass is more centrally concentrated. Note that the distribution is normalized such that $\int_0^1 N_\beta(e) de = 1$.

the value of β and is helpful in interpreting the results of more realistic models in the next section.

3 ECCENTRICITY DISTRIBUTION OF HALO STARS

Our formulation in the previous section can apply to more general cases of mass distribution, including the isochrone model and the NFW model that could form two ends covering in-between any realistic cases of mass distribution of dark halo.

3.1 Energy-dependent eccentricity distribution $n_\beta(\varepsilon, e)$ for the isochrone model

The gravitational potential of the isochrone model (Hénon 1959) is given by

$$V(r) = -\frac{GM}{b + \sqrt{b^2 + r^2}}, \quad (28)$$

where M is the total mass and b is the scale length parameter. Obviously, the asymptotic form in the limit of $r \gg b$ or $r \ll b$ approaches the point mass model or the homogeneous model, respectively. Thus, this model, though not explaining the flat rotation curve of the galaxy disk at greater distances from the galaxy center, is important to study the intermediate case of mass distribution by adjusting the scale size of the central core. Furthermore, the isochrone model is particularly valuable, because fully analytic expression of $n_\beta(E, e)$ can be obtained.

Provided $b \neq 0$, we define useful dimensionless variables and effective potential as follows:

$$x \equiv \frac{r}{b}, \quad \varepsilon \equiv \frac{2bE}{GM}, \quad \lambda \equiv \frac{2L^2}{bGM}, \quad (29)$$

and

$$\Phi_{\text{eff}}(\lambda; x) \equiv \frac{2b}{GM} \left[V(r) + \frac{L^2}{2r^2} \right] = -\frac{2}{1 + \sqrt{1 + x^2}} + \frac{\lambda}{2x^2}. \quad (30)$$

Equation (3) then reads

$$\varepsilon x^2 + 2\sqrt{1 + x^2} - \left(2 + \frac{\lambda}{2} \right) = 0. \quad (31)$$

This equation has two real and positive solutions if and only if

$$-1 < \varepsilon < 0 \quad \text{and} \quad 0 < \lambda < \lambda_{\text{cir}} \equiv \frac{2(1 + \varepsilon)^2}{-\varepsilon}. \quad (32)$$

We denote the two solutions x_{peri} and x_{apo} , and use of them gives the relevant quantities in terms of ε and e :

$$T_r = 2\pi \sqrt{\frac{b^3}{GM}} (-\varepsilon)^{-\frac{3}{2}}, \quad (33)$$

$$L^2 = \frac{bGM}{2} \left(-4 - \frac{2}{\varepsilon} + \frac{1}{\varepsilon^2} \left[(1 + e^4) - (1 + e^2) \sqrt{(1 - e^2)^2 + 4\varepsilon^2 e^2} \right] \right), \quad (34)$$

and

$$\left(\frac{\partial L^2}{\partial e} \right)_E = -bGM(-\varepsilon)^{-1} \times \frac{(1 - e^2)}{e^3} \left[\frac{1 + 2\varepsilon^2 e^2 + e^4}{\sqrt{(1 - e^2)^2 + 4\varepsilon^2 e^2}} - (1 + e^2) \right]. \quad (35)$$

Consequently, after tedious algebra, we succeed for the first

time to obtain analytic expression of $n_\beta(\varepsilon, e)$ as follows:

$$\begin{aligned} n_\beta(\varepsilon, e) &= 8\pi^3 \sqrt{b^5 GM} (-\varepsilon)^{-\frac{5}{2}} \\ &\times \frac{(1 - e^2)}{e^3} \left[\frac{1 + 2\varepsilon^2 e^2 + e^4}{\sqrt{(1 - e^2)^2 + 4\varepsilon^2 e^2}} - (1 + e^2) \right] \\ &\times \left[\frac{bGM}{2} \left(-4 - \frac{2}{\varepsilon} + \frac{1}{\varepsilon^2} \left[(1 + e^4) - (1 + e^2) \sqrt{(1 - e^2)^2 + 4\varepsilon^2 e^2} \right] \right) \right]^{-\beta}. \end{aligned} \quad (36)$$

We see that $n_\beta(\varepsilon, e)$ is not separable in ε and e . Therefore, unlike the point mass and homogeneous models, the shape of $n_\beta(\varepsilon, e)$ depends on ε as well as β . Accordingly, derivation of $N_\beta(e)$ needs full numerical integration of $n_\beta(\varepsilon, e)$ over ε with the weight function $g(\varepsilon)$ specified.

When $\beta = 0$, by taking a limit of ε , we obtain

$$\lim_{\varepsilon \rightarrow -0} n_{\beta=0}(\varepsilon, e) \propto e(-\varepsilon)^{-\frac{5}{2}}, \quad (37)$$

and

$$\lim_{\varepsilon \rightarrow -1} n_{\beta=0}(\varepsilon, e) \propto \frac{e(1 - e^2)}{(1 + e^2)^3} (1 + \varepsilon). \quad (38)$$

These shapes of e -distribution exactly coincide with those in equations (37) and (38), respectively. As understood from the definition of $\varepsilon [\equiv 2bE/(GM)]$, the limit of $\varepsilon \rightarrow 0$ corresponds to $b \rightarrow 0$ with E and M fixed, which is equivalent to taking a limit to the point mass model. Likewise, the limit of $\varepsilon \rightarrow -1$ corresponds to $b \rightarrow \infty$, otherwise such limit of ε is not attained with E and M fixed, which is equivalent to taking a limit to the homogeneous model.

The shapes of $n_\beta(\varepsilon, e)$ for several values of ε and β are shown in Figure 3. For any value of β , there is a general trend such that eccentric orbits become more and more dominant as ε increases. However, a marked β -dependence shows up in the shape of $n_\beta(\varepsilon, e)$.

When $\beta \lesssim 0.6$, $n_\beta(\varepsilon, e)$ has a hump-like e -distribution with a peak at $e = e_{\text{peak}}$. On the other hand, when $0.6 \lesssim \beta \leq 1$, $n_\beta(\varepsilon, e)$ has a monotonically increasing e -distribution with a peak at $e = 1$. In particular, for $\beta \approx 0.6$ and $\varepsilon \simeq -1$, $n_\beta(\varepsilon, e)$ shows something like a trapezoidal shape, similar to the case of $\beta \approx 0.6$ for the homogeneous model (left panel of Figure 1). Furthermore, for $\beta > 0.8$, highly eccentric orbits prominently dominate in the e -distribution.

In order to understand the situation differently, the plots of e_{peak} at which the e -distribution is peaked for several values of ε and β are shown on the left panel of Figure 5. Here, by taking a limit of ε , we can easily confirm, through comparison of this figure with Figure 1, that

$$\lim_{\varepsilon \rightarrow -0} e_{\text{peak}}(\beta, \varepsilon) = e_{\text{peak}}^{\text{pm}}(\beta), \quad (39)$$

and

$$\lim_{\varepsilon \rightarrow -1} e_{\text{peak}}(\beta, \varepsilon) = e_{\text{peak}}^{\text{hom}}(\beta), \quad (40)$$

where superscripts ‘pm’ and ‘hom’ correspond to the point mass model and the homogeneous model, respectively. More generally, when $\beta > 0.6$, we see that $e_{\text{peak}} = 1$ for any value of ε . On the other hand, when $\beta \leq 0.5$, we see that e_{peak} is an increasing function of both ε and β .

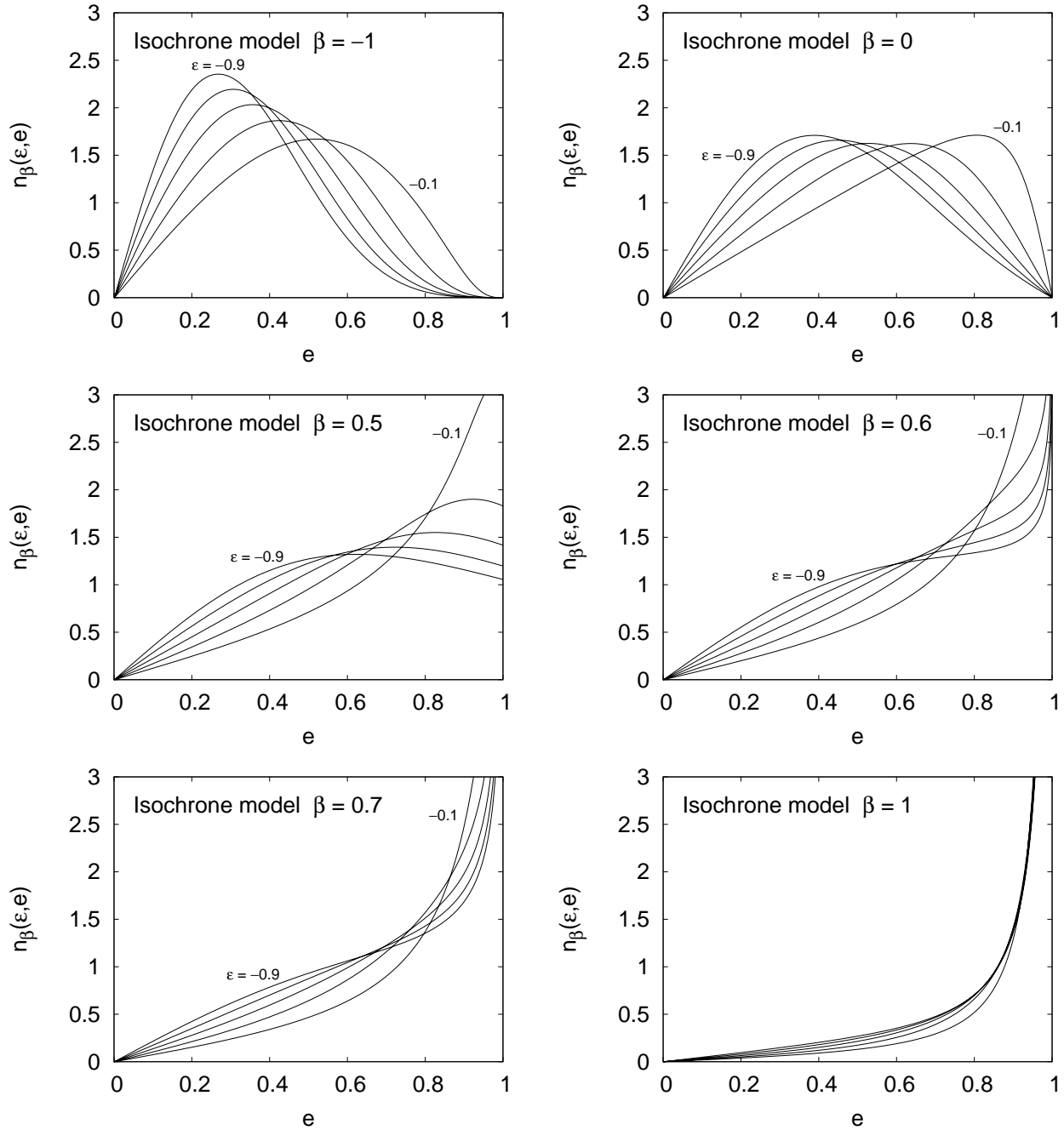


Figure 3. Energy-dependent differential distribution of stellar orbital eccentricity $n_{\beta}(\varepsilon, e)$ for the isochrone model. In different panels for different values of velocity anisotropy parameter β , shown by lines are the results for dimensionless energy $\varepsilon = -0.9, -0.7, \dots, -0.1$, in steps of 0.2. Note that $n_{\beta}(\varepsilon, e)$ is normalized such that $\int_0^1 n_{\beta}(\varepsilon, e) de = 1$. By this normalization, the inclination of $n_{\beta}(\varepsilon, e)$ at $e = 0$, which is lower for smaller $|\varepsilon|$, helps identify each line.

3.2 Energy-dependent eccentricity distribution $n_{\beta}(\varepsilon, e)$ for the NFW model

Cosmological simulations have been run to reconstruct galaxies from the primordial density fluctuations in the universe. These numerical results have shown that the dark halo has a universal shape of so-called NFW density profile that has little dependence on the cosmology (Navarro, Frenk &

White 1997), such as

$$\rho(r) = \rho_0 \cdot \frac{a^3}{r(a+r)^2}, \quad (41)$$

where a is the scale length parameter. This density profile behaves as $\rho \propto 1/r$ for $r \ll a$, while $\rho \propto 1/r^3$ for $r \gg a$. The associated gravitational potential is of the form

$$V(r) = -4\pi G \rho_0 a^3 \frac{\ln(1+r/a)}{r}. \quad (42)$$

Provided $a \neq 0$, we define dimensionless variables and effective potential as follows:

$$x \equiv \frac{r}{a}, \quad \varepsilon \equiv \frac{E}{4\pi G\rho_0 a^2}, \quad \lambda \equiv \frac{L^2}{4\pi G\rho_0 a^4}, \quad (43)$$

and

$$\Phi_{\text{eff}}(\lambda; x) \equiv \frac{1}{4\pi G\rho_0 a^2} \left[V(r) + \frac{L^2}{2r^2} \right] \equiv -\frac{\ln(1+x)}{x} + \frac{\lambda}{2x^2}. \quad (44)$$

Equation (3) then reads

$$\varepsilon x^2 + x \ln(1+x) - \frac{\lambda}{2} = 0. \quad (45)$$

This equation indicates a one-to-one correspondence between (ε, λ) and (ε, e) , and allows two real and positive solutions if and only if

$$-1 < \varepsilon < 0 \quad \text{and} \quad 0 < \lambda < \lambda_{\text{cir}} \equiv x_c \ln(1+x_c) - \frac{x_c^2}{1+x_c}, \quad (46)$$

where x_c is the solution for

$$-2\varepsilon = \frac{\ln(1+x)}{x} + \frac{1}{1+x}. \quad (47)$$

We denote the two solutions x_{peri} and x_{apo} ($x_{\text{apo}} > x_{\text{peri}}$), and use of them gives

$$T_r = \sqrt{\frac{1}{2\pi G\rho_0}} \int_{x_{\text{peri}}}^{x_{\text{apo}}} \frac{xdx}{\sqrt{\varepsilon x^2 + x \ln(1+x) - \frac{\lambda}{2}}}, \quad (48)$$

$$L^2 = 8\pi G\rho_0 a^4 [\varepsilon x_i^2 + x_i \ln(1+x_i)] \quad (x_i = x_{\text{peri}} \text{ OR } x_{\text{apo}}), \quad (49)$$

and

$$\left(\frac{\partial L^2}{\partial e} \right)_E = -4\pi G\rho_0 a^4 (x_{\text{apo}} + x_{\text{peri}})^2 \times \left[\frac{x_{\text{apo}}}{x_{\text{peri}} \left(2\varepsilon + \frac{1}{1+x_{\text{peri}}} \right) + \ln(1+x_{\text{peri}})} - \frac{x_{\text{peri}}}{x_{\text{apo}} \left(2\varepsilon + \frac{1}{1+x_{\text{apo}}} \right) + \ln(1+x_{\text{apo}})} \right]^{-1}. \quad (50)$$

We see that $n_\beta(\varepsilon, e)$ does not allow analytic expression in terms of ε and β . Accordingly, derivation of $n_\beta(\varepsilon, e)$, as well as $N_\beta(e)$ with the weight function $g(\varepsilon)$, needs full numerical integration for the NFW model.

The results of $n_\beta(\varepsilon, e)$ for several values of ε and β are shown in Figure 4. The plots of e_{peak} at which the e -distribution is peaked for several values of ε and β are shown on the right panel of Figure 5. Here, similarly to the isochrone model, by taking a limit of ε , we can easily confirm that

$$\lim_{\varepsilon \rightarrow -0} e_{\text{peak}}(\beta, \varepsilon) = e_{\text{peak}}^{\text{pm}}(\beta), \quad (51)$$

and

$$\lim_{\varepsilon \rightarrow -1} e_{\text{peak}}(\beta, \varepsilon) = e_{\text{peak}}^{\text{lp}}(\beta), \quad (52)$$

where superscripts ‘pm’ and ‘lp’ correspond to the point

mass model and the linear potential model described in Appendix B.1, respectively.

Except for slight shift of the e -distribution to have more weight at higher e , overall behavior of $n_\beta(\varepsilon, e)$ for the NFW model is very similar to the isochrone model. Such slight shift occurs, because the mass is little more centrally concentrated in the NFW model compared with the isochrone model.

The insensitivity to the choice of gravitational potential, as far as it remains realistic, is encouraging, especially when our theoretical e -distribution is to be compared with that observed for stars in the Milky Way halo.

3.3 Results of $N_\beta(e)$

In the previous subsections, we have derived the E -dependent form of $n_\beta(E, e)$ for the respective models of isochrone and NFW. In order to obtain their eccentricity distribution $N_\beta(e)$ in equation (9), we have to specify the weight function of $g(E)$ which can in principle be derived in a self-consistent way (Lynden-Bell 1962, 1963). Here, instead of entering into robustness, however, we take a simple approximation of $g(E)$ as having the form:

$$g(E) = A \exp\left(-\frac{E}{\sigma^2}\right), \quad (53)$$

where A is a constant and σ stands for the radial velocity dispersion $\sigma_r \sim 150 \text{ km s}^{-1}$ for the Milky Way halo stars (e.g. Yoshii & Saio 1979; Chiba & Beers 2000, 2001).

We can imagine that halo stars traveling far distantly from the galaxy center with near-zero energy would be captured by adjacent dark halo. Thus, it is reasonable to introduce a truncation energy E_t above which $g(E)$ should vanish.

The NFW model provides a direct reason to include E_t in the analysis. The mass of dark halo within the radius r is naively given by

$$M(r) = 4\pi\rho_0 a^3 \left[\ln\left(1 + \frac{r}{a}\right) - \frac{r/a}{1+r/a} \right] \quad (54)$$

and diverges in the limit of large r . In fact, numerical simulations indicate that the NFW density profile applies only inside a certain boundary radius but does not apply beyond it because of the existence of adjacent dark halos. Such a boundary usually used is the virial radius r_{200} within which the averaged density is equal to 200 times the critical density of the universe and the effects by adjacent dark halos are negligible. Thus, it is reasonable to place E_t at $V(r_{200})$ and assume that while halo stars with $E < E_t$ stay in the system, those with $E > E_t$ could be unbound and leave the system.

From all these considerations, we examine how $N_\beta(e)$ would be modified with E_t taken into account in the analysis. Here, we set E_t equal to the potential energy $V(r_{200})$ and write it in the dimensionless form:

$$\varepsilon_t = -\frac{\ln(1+c)}{c}, \quad (55)$$

where c is the concentration parameter defined as $c \equiv r_{200}/a$. Use of the kinematic data of the blue horizontal branch stars in the Milky Way halo and some CDM simulations of a halo of $M(r_{200}) \sim 10^{12} M_\odot$ as massive as the Milky

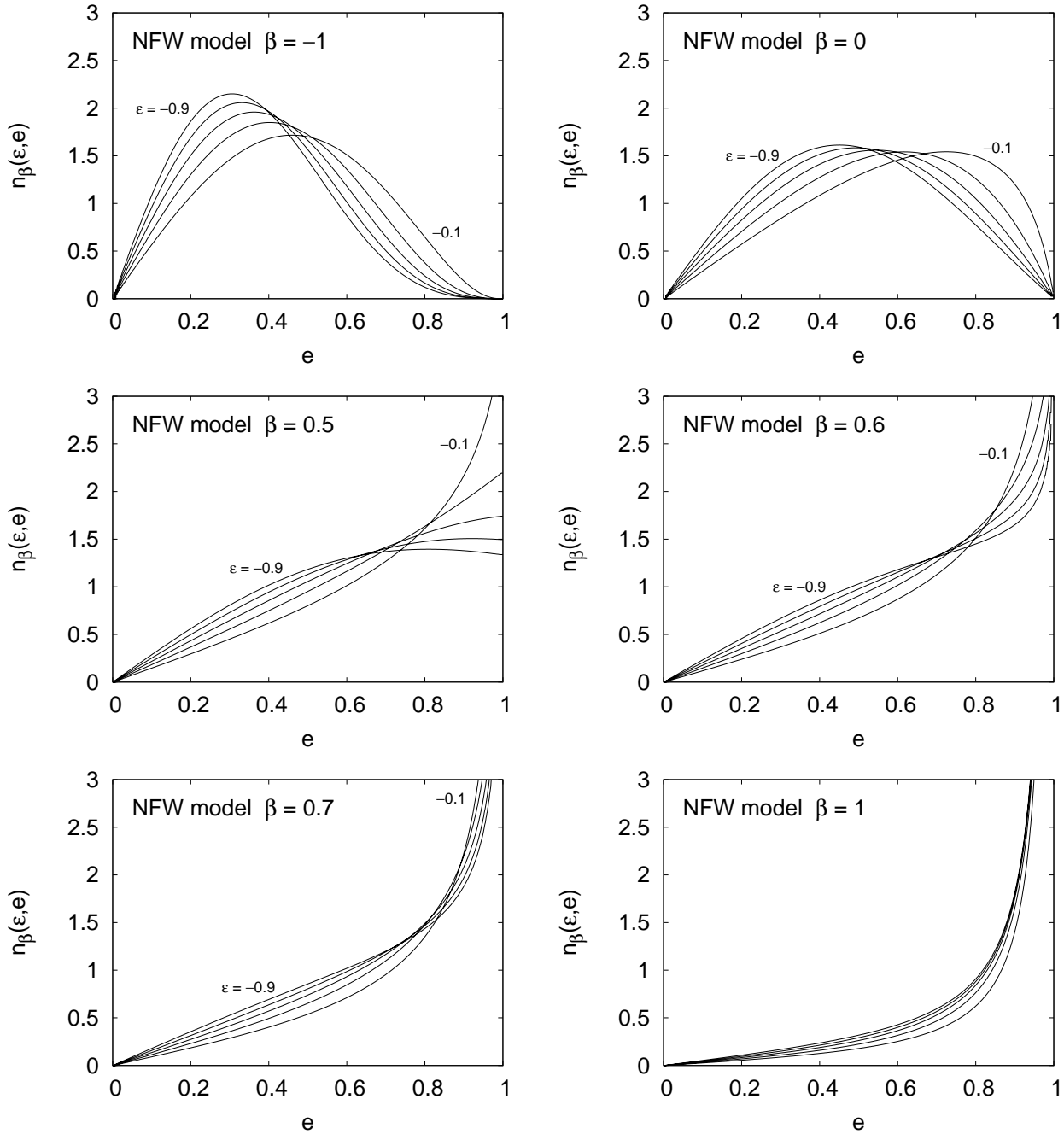


Figure 4. Energy-dependent differential distribution of stellar orbital eccentricity $n_\beta(\varepsilon, e)$ for the NFW model. Others are the same as in Figure 3.

Way halo gives $c = 3.9 - 12.5$ (Xue et al. 2008), which corresponds to $\varepsilon_t = -0.4$ to -0.2 . Thus, a choice of this range of ε_t , together with $\beta = 0.5 - 0.7$ (cf. section 2.2), would be appropriate for our analysis of the Milky Way halo.

We have repeated the calculations of $N_\beta(e)$ for several values of σ and ε_t in the integration of $n_\beta(\varepsilon, e)$ over ε in equation (9), and find that $N_\beta(e)$ is insensitive to σ but sensitive to ε_t . The shape of $N_\beta(e)$ is almost the same as that of $n_\beta(\varepsilon_t, e)$. This is because $n_\beta(\varepsilon_t, e)$ significantly contributes to the integration of $n_\beta(\varepsilon, e)$. For example, in a particular case of $\beta = 0$ for the isochrone model, we clearly see such a

situation from the explicit expression:

$$\int_0^1 n_{\beta=0}(\varepsilon, e) de = 8\pi^3 \sqrt{GMb^5} (1 + \varepsilon)^2 (-\varepsilon)^{-\frac{5}{2}}. \quad (56)$$

Using the typical combinations of $(\beta, \varepsilon_t) = (0.5, -0.2)$, $(0.5, -0.4)$, $(0.7, -0.2)$, and $(0.7, -0.4)$ that more or less agree with observations of the Milky Way halo, the results of $N_\beta(e)$ for both the isochrone and NFW models are shown in Figure 6. We see from this figure that as far as reasonable values of β and ε_t are adopted, the resulting shape of $N_\beta(e)$ should be almost linearly proportional to e , except

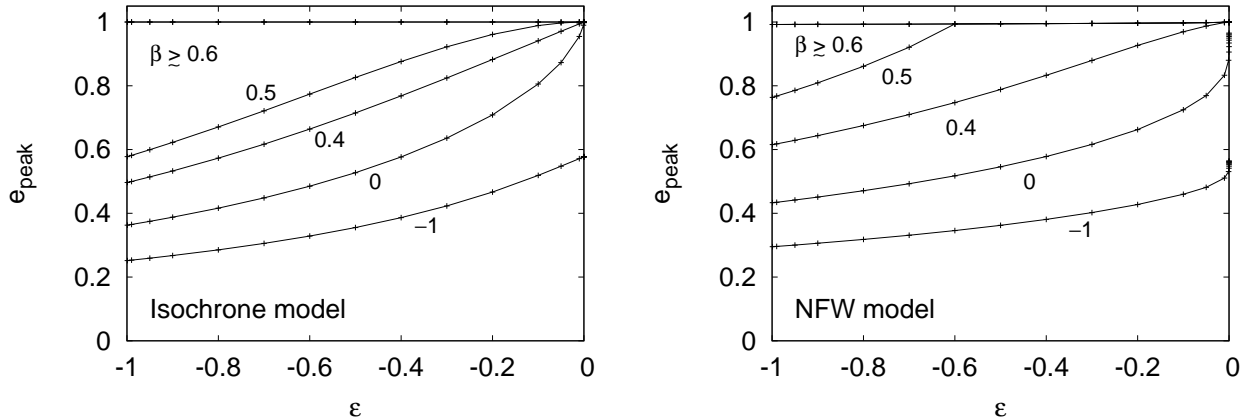


Figure 5. The peak eccentricity e_{peak} as a function of dimensionless energy ϵ for the isochrone model (left panel) and the NFW model (right panel). The results are shown by lines for different values of velocity anisotropy parameter β .

for the deviation only at $e > 0.7$. This is largely regardless of adopting either the isochrone model or the NFW model. Thus, if the dominant component of the Milky Way halo is in dynamical equilibrium, the total eccentricity distribution of stellar halo is expected to have a linear trend at $e < 0.7$ similar to our results. On the other hand, the behavior of predicted $N(e)$ at $e > 0.7$, which still shows little difference between the isochrone and NFW models, is sensitive to β and ϵ_t . Consequently, such sensitivity can be used for a consistency check of the assumed form of $f(E, L)$. These predictions in the separate regions of $e < 0.7$ and $e > 0.7$ are testable, given that large kinematical data of halo stars are available at present from the SEGUE project or in the near future from the Gaia project.

4 SUMMARY AND DISCUSSION

Hierarchical clustering scenarios of galaxy formation suggest that the major merger of at least several subhalos with comparable masses would occur at the last stage of galaxy formation. This last major merger would cause the violent relaxation of halo stars and make them in dynamical equilibrium with a dark halo. Based on the assumptions that approximate such a status just after the last violent relaxation (section 1), we have presented theoretical predictions of $N(e)$ for halo stars. This predicted $N(e)$ should be observed for the Milky Way halo if it is an isolated system and the subsequent variation of the potential is quiescent enough to conserve the eccentricity of each star.

However, recent nearby observations suggest that at least some part of the Milky Way halo may have originated from accreted satellites, which possibly deviates the observed $N(e)$ from our predictions. For example, if infalling satellites break up and spread their member stars into the field, these stars would show peculiar eccentricity distribution which necessarily imprints the initial condition of the progenitor satellites. In addition, if such satellites locally disturb the halo potential, some *in-situ* halo stars may have altered their orbits (e.g. Zolotov et al. 2009). With an invention of segregating *in-situ* halo stars from infalling stars,

we might be able to well understand the nature of accretion and distortion of satellites.

Numerous authors subdivided halo stars into some ‘components’ and examined the correlations between chemistry, age and kinematics of stars in each component. Carollo et al. (2010) obtained reliable eccentricities for $\sim 10,000$ halo stars within 4 kpc of the sun and decomposed them into the inner and outer halo components having distinct eccentricity distributions from each other. Since their sample is *local* and is inherently biased in favour of stars that stay longer in the surveyed region, our formalism, which is designed to predict $N(e)$ of the whole stellar halo, has to be modified for the purpose of fair comparison with their data. Through proper incorporation of effects of such a bias, we can still predict $N(e)$ for a *local* sample by fully taking into account a probability of finding each of halo stars in the surveyed region. This will be done in a separate paper in preparation. On the other hand, our formalism can directly apply to a *global*, and therefore less biased, sample of halo stars with reliable orbital eccentricities, such as those from next generation surveys including the Gaia mission. In either case, the analytical approach in the present paper certainly forms a basis that serves as a useful tool for analysing the kinematics of the stellar halo.

Large, unbiased database of halo stars would enable us to test whether a given component is in dynamical equilibrium by comparing the observed and predicted shape of $N(e)$. Such comparison would hopefully discover some relaxed components, and their adiabatically conserved shape of $N(e)$ would carry some useful information of the physics of violent relaxation. Moreover, the spatial distribution of these relaxed components would enable us to see how far out in the halo the violent relaxation has exerted and how strongly it has affected the stellar halo. If the information of last violent relaxation, yet to be known observationally, is gained in this way, more precise assessment to the early evolution of the Milky Way would be possible, and our understanding of its formation would greatly be advanced.

Our current calculations of $N(e)$ are certainly very simple and can be improved by using more realistic assumptions. For example, we can modify our analysis to allow

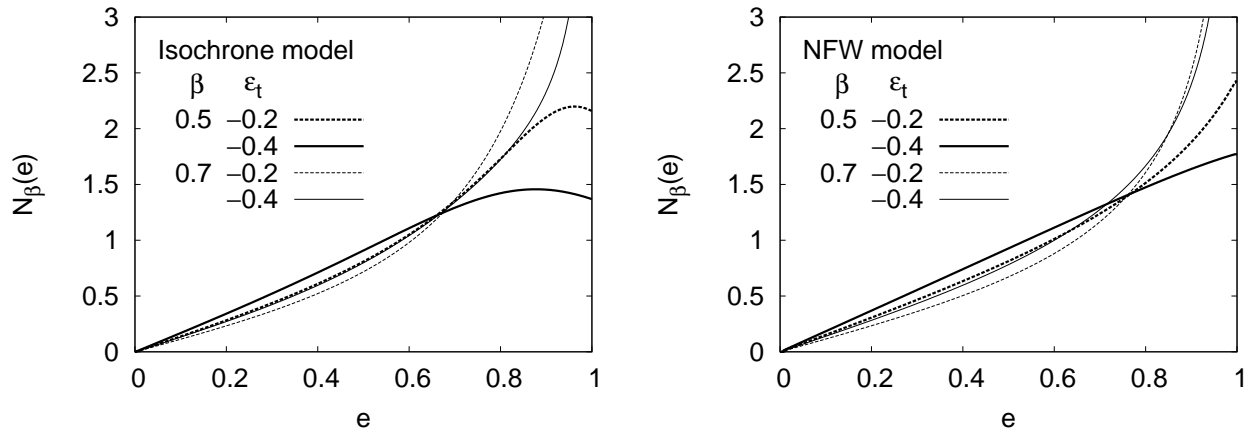


Figure 6. Differential distribution of stellar orbital eccentricity $N_\beta(e)$ for the isochrone model (left panel) and the NFW model (right panel). Adopted combinations of (β, ε_t) more or less agree with observations of the Milky Way halo. Note that the normalization factor of $N_\beta(e)$ is arbitrarily chosen so that the nearly linear trend up to $e \approx 0.7$ is clearly seen.

axisymmetric potentials including a disk-like component as well as a bulge. Preliminary analysis has confirmed that inclusion of a disk-like component would cause no significant change in the linear trend of $N(e)$ described in section 3.3, which will be discussed in a separate paper. Also, our choice of $f(E, L)$ having the form in equation (4) has to be extended to allow the radial dependence of $\beta(r)$. Further elaborate modeling of $N(e)$ with these theoretical improvements, when applied to future large survey of halo stars, would then provide a promising way of unraveling mysteries of the galaxy formation and evolution in a paradigm of hierarchical clustering in the Λ CDM cosmology.

ACKNOWLEDGMENTS

We thank Beers, T., Carollo, D., Minezaki, T., Tsujimoto, T., and Yamagata, T. for useful discussions and suggestions.

REFERENCES

- Beers, T. C., Chiba, M., Yoshii, Y., Platais, I., Hanson, R. B., Fuchs, B., & Rossi, S. 2000, *AJ*, 119, 2866
- Bertschinger, E. 1998, *ARA&A*, 36, 599
- Binney, J., & Tremaine, S. 2008, *Galactic Dynamics*, 2nd edn. Princeton Univ. Press, Princeton, NJ
- Blumenthal, G. R., Faber, S. M., Primack, J. R., & Rees, M. J. 1984, *Nature*, 311, 517
- Bond, N. A., Ivezić, Z., Sesar, B., Juric, M., & Munn, J. 2009, arXiv:0909.0013
- Carollo, D., et al. 2007, *Nature*, 450, 1020
- Carollo, D., et al. 2010, *ApJ*, 712, 692
- Chiba, M., & Beers, T. C. 2000, *AJ*, 119, 2843
- Chiba, M., & Beers, T. C. 2001, *ApJ*, 549, 325
- Cole, S., et al. 2005, *MNRAS*, 362, 505
- Dunkley, J., et al. 2009, *ApJS*, 180, 306
- Eggen, O. J., Lynden-Bell, D., & Sandage, A. R. 1962, *ApJ*, 136, 748
- Ghigna, S., Moore, B., Governato, F., Lake, G., Quinn, T., & Stadel, J. 2000, *ApJ*, 544, 616

- Gilmore, G., Wyse, R. F. G., & Kuijken, K. 1989, *ARA&A*, 27, 555
- Helmi, A., White, S. D. M., & Springel, V. 2003, *MNRAS*, 339, 834
- Hénon, M. 1959, *Annales d’Astrophysique*, 22, 126
- Lynden-Bell, D. 1960, *MNRAS*, 120, 204
- Lynden-Bell, D. 1962, *MNRAS*, 124, 1
- Lynden-Bell, D. 1963, *The Observatory*, 83, 23
- Lynden-Bell, D. 1967, *MNRAS*, 136, 101
- Moore, B., Ghigna, S., Governato, F., Lake, G., Quinn, T., Stadel, J., & Tozzi, P. 1999, *ApJ*, 524, L19
- Navarro, J. F., Frenk, C. S., & White, S. D. M. 1997, *ApJ*, 490, 493
- Ostriker, J. P. 1993, *ARA&A*, 31, 689
- Smith, M. C., et al. 2009, *MNRAS*, 399, 1223
- Valluri, M., Vass, I. M., Kazantzidis, S., Kravtsov, A. V., & Bohn, C. L. 2007, *ApJ*, 658, 731
- White, S. D. M., & Rees, M. J. 1978, *MNRAS*, 183, 341
- Xue, X. X., et al. 2008, *ApJ*, 684, 1143
- Yoshii, Y., & Saio, H. 1979, *PASJ*, 31, 339
- Zolotov, A., Willman, B., Brooks, A. M., Governato, F., Brook, C. B., Hogg, D. W., Quinn, T., & Stinson, G. 2009, *ApJ*, 702, 1058

APPENDIX A: ALLOWED REGION OF (E, L) FOR BOUND ORBIT

A steady, bound orbit in a gravitational potential $V(r)$ generated by a density distribution $\rho(r)$ is only possible in a subset of energy E and angular momentum L that allows two real and positive solutions for equation (3). We discuss such an allowed region of (E, L) in this appendix. We begin with the effective potential

$$V_{\text{eff}}(L; r) = V(r) + \frac{L^2}{2r^2}. \quad (\text{A1})$$

Then, from the definition, we obtain

$$\left(\frac{\partial}{\partial r} V_{\text{eff}}(L; r) \right)_L = \frac{1}{r^3} [GM(r)r - L^2], \quad (\text{A2})$$

where $M(r)$ is the total mass inside the radius r . Since $GM(r)r$ is a monotonically increasing function of r and it satisfies

$$\lim_{r \rightarrow 0} [GM(r)r] = 0, \quad \text{and} \quad \lim_{r \rightarrow \infty} [GM(r)r] = \infty, \quad (\text{A3})$$

there always exists an radius $r_c = r_c(L)$ for which $GM(r_c)r_c = L^2$, thus yielding

$$\left(\frac{\partial}{\partial r} V_{\text{eff}}(L; r) \right)_L \geq 0, \quad \text{if } r \geq r_c. \quad (\text{A4})$$

Since we have

$$\frac{d}{d(L^2)} r_c = [G(4\pi r_c^3 \rho(r_c) + M(r_c))]^{-1} > 0, \quad (\text{A5})$$

and

$$\frac{d}{d(L^2)} V_{\text{eff}}(L; r_c(L)) = \frac{1}{2r_c^2} > 0, \quad (\text{A6})$$

the allowed range of E with L fixed can be expressed as

$$V_{\text{eff}}(L; r_c(L)) < E < 0. \quad (\text{A7})$$

Here, we define the zero of $V(r)$ so that $\lim_{r \rightarrow \infty} V(r) = 0$. Thus, for any given L , we obtain

$$\lim_{r \rightarrow \infty} V_{\text{eff}}(L; r) = 0, \quad (\text{A8})$$

which validates that the upper bound of inequality (A7) should be zero. As for the allowed region of L when E is fixed, we obtain

$$0 < L < L_{\text{cir}}(E), \quad (\text{A9})$$

for which $L_{\text{cir}}(E)$ is the solution of

$$E = V_{\text{eff}}(L_{\text{cir}}; r_c(L_{\text{cir}})). \quad (\text{A10})$$

APPENDIX B: OTHER MODELS OF TRUNCATED MASS DISTRIBUTION

We present the derivation of $N_\beta(e)$ for two models of truncated power-law mass distribution:

$$\rho(r) = \begin{cases} \frac{(3-\gamma)M}{4\pi r_t^3} \left(\frac{r}{r_t}\right)^{-\gamma}, & (\gamma < 3) \quad \text{if } r < r_t \\ 0, & \text{otherwise,} \end{cases} \quad (\text{B1})$$

where M is the total mass of the dark halo and r_t is the truncation radius. We note that the truncated homogeneous model presented in section 2.3.2 is a special case of $\gamma = 0$ in equation (B1).

B1 Linear potential model ($\gamma = 1$)

The NFW density profile has a central cusp and behaves like $\rho(r) \propto 1/r$ in the limit of Small r . This density profile corresponds to $\gamma = 1$ in equation (B1), and we have

$$\rho(r) = \begin{cases} \frac{M}{2\pi r_t^3} \left(\frac{r}{r_t}\right)^{-1}, & \text{if } r < r_t \\ 0, & \text{otherwise.} \end{cases} \quad (\text{B2})$$

The gravitational potential arising from this density profile is given by

$$V(r) = \begin{cases} -\frac{2GM}{r_t} + \frac{GM}{r_t} \left(\frac{r}{r_t}\right), & \text{if } r < r_t \\ -\frac{GM}{r}, & \text{otherwise,} \end{cases} \quad (\text{B3})$$

and we will refer to this potential a ‘truncated linear potential.’ We consider only stars with $E < E_t \equiv -GM/r_t$, which guarantees the stars to be confined inside the truncated radius r_t . Thus, bound orbits within the truncated sphere are allowed if $E_{\text{min}} < E < E_t$ where we note $E_{\text{min}} \equiv 2E_t$. In this limited range of E , there are two real and positive solutions for equation (3), or equivalently,

$$2GMr_t \left(\frac{r}{r_t}\right)^3 - 2r_t^2 (E - E_{\text{min}}) \left(\frac{r}{r_t}\right)^2 + L^2 = 0, \quad (\text{B4})$$

if and only if

$$0 < D < 2, \quad (\text{B5})$$

where

$$D = \frac{27G^2 M^2 L^2}{4r_t^4 (E - E_{\text{min}})^3}. \quad (\text{B6})$$

In this allowed region, two real and positive solutions for equation (B4) are as follows:

$$r_i = \frac{2r_t^2}{3GM} (E - E_{\text{min}}) x_i \quad (i = \text{apo or peri}; r_{\text{apo}} > r_{\text{peri}}), \quad (\text{B7})$$

with x_{apo} and x_{peri} given, respectively, by

$$x_{\text{apo}} = \frac{1}{2} + \cos \theta, \quad \text{and} \quad x_{\text{peri}} = \frac{1}{2} + \cos \left[\frac{4\pi}{3} + \theta \right], \quad (\text{B8})$$

thus

$$e = \frac{\cos \theta - \cos \left[\frac{4\pi}{3} + \theta \right]}{1 + \cos \theta + \cos \left[\frac{4\pi}{3} + \theta \right]}, \quad (\text{B9})$$

where

$$\theta = \begin{cases} \frac{1}{3} \tan^{-1} \left(\frac{\sqrt{2D-D^2}}{1-D} \right), & \text{if } 0 < D < 1 \\ \frac{1}{3} \left[\tan^{-1} \left(\frac{\sqrt{2D-D^2}}{1-D} \right) + \pi \right], & \text{if } 1 < D < 2. \end{cases} \quad (\text{B10})$$

Consequently, D has a one-to-one correspondence to e , so with θ , x_{apo} , and x_{peri} . Use of these quantities gives

$$L^2 = \frac{4r_t^4 D}{27G^2 M^2} (E - E_{\text{min}})^3, \quad (\text{B11})$$

$$T_r = 2\sqrt{3} r_t^2 \frac{\sqrt{E - E_{\text{min}}}}{GM} \int_{x_{\text{peri}}}^{x_{\text{apo}}} \frac{xdx}{\sqrt{-x^3 + \frac{3}{2}x^2 - \frac{D}{4}}}, \quad (\text{B12})$$

and

$$\begin{aligned} \left(\frac{\partial L^2}{\partial e} \right)_E &= -\frac{4r_t^4 \sqrt{2D-D^2}}{9G^2 M^2} (E - E_{\text{min}})^3 \\ &\times \frac{(1 + \cos \theta + \cos \left[\frac{4\pi}{3} + \theta \right])^2}{\sin \theta (1 + 2 \cos \left[\frac{4\pi}{3} + \theta \right]) - \sin \left[\frac{4\pi}{3} + \theta \right] (1 + 2 \cos \theta)}. \end{aligned} \quad (\text{B13})$$

By these expressions, we obtain

$$n_\beta(E, e) = 24\sqrt{3}\pi^2 \frac{r_t^2}{GM} \left(\frac{4r_t^4}{27G^2M^2} \right)^{1-\beta} \\ \times D^{-\beta} \sqrt{2D - D^2(E - E_{\min})}^{\frac{7}{2}-3\beta} \\ \times \frac{(1 + \cos\theta + \cos[\frac{4\pi}{3} + \theta])^2}{\sin\theta (1 + 2\cos[\frac{4\pi}{3} + \theta]) - \sin[\frac{4\pi}{3} + \theta] (1 + 2\cos\theta)} \\ \times \int_{x_{\text{peri}}}^{x_{\text{apo}}} \frac{xdx}{\sqrt{-x^3 + \frac{3}{2}x^2 - \frac{D}{4}}}. \quad (\text{B14})$$

Since θ , D , x_{apo} , and x_{peri} depend only on e , $n_\beta(E, e)$ is separable in E and e , so that

$$N_\beta(e) = 24\sqrt{3}\pi^2 \frac{r_t^2}{GM} \left(\frac{4r_t^4}{27G^2M^2} \right)^{1-\beta} \\ \times D^{-\beta} \sqrt{2D - D^2} \left[\int g(E)(E - E_{\min})^{\frac{7}{2}-3\beta} dE \right] \\ \times \frac{(1 + \cos\theta + \cos[\frac{4\pi}{3} + \theta])^2}{\sin\theta (1 + 2\cos[\frac{4\pi}{3} + \theta]) - \sin[\frac{4\pi}{3} + \theta] (1 + 2\cos\theta)} \\ \times \int_{x_{\text{peri}}}^{x_{\text{apo}}} \frac{xdx}{\sqrt{-x^3 + \frac{3}{2}x^2 - \frac{D}{4}}}. \quad (\text{B15})$$

Therefore, the shape of $N_\beta(e)$ is not affected by E or $g(E)$, like the point mass model and the truncated model with any γ . The results of $N_\beta(e)$ in the linear potential model are shown on the left panel of Figure B1. We see that $N_\beta(e)$ is a monotonically increasing e -distribution for $0.52 < \beta < 1$, and $N_\beta(e)$ has a hump-like e -distribution with a single peak for $\beta < 0.5$. In particular, $N_{\beta=0}(e)$ reaches its maximum at $e_{\text{peak}} = 0.43$. In the intermediate range of $0.5 < \beta < 0.52$, $N_\beta(e)$ shows something like a trapezoidal e -distribution, which shows a monotonically increasing e -distribution for $0 < e < e_{\text{peak}}$ and a more or less flat behavior for $e_{\text{peak}} < e < 1$, where $e_{\text{peak}} \simeq 0.8$.

B2 Singular isothermal model ($\gamma = 2$)

One of the most strong constraints on the gravitational potential of the halo is that it has to be consistent with the observed flat rotation curve of galaxy disk. In this sense, the truncated singular isothermal model, which automatically reproduces the flat rotation curve in the radial range of $0 < r < r_t$, is said to be one of the simple and realistic models. The density profile of this model is given by

$$\rho(r) = \begin{cases} \frac{M}{4\pi r_t^3} \left(\frac{r}{r_t} \right)^{-2}, & \text{if } r < r_t \\ 0, & \text{otherwise,} \end{cases} \quad (\text{B16})$$

which corresponds to $\gamma = 2$ in equation (B1). The gravitational potential arising from this density profile is given by

$$V(r) = \begin{cases} -\frac{GM}{r_t} + \frac{GM}{r_t} \ln\left(\frac{r}{r_t}\right), & \text{if } r < r_t \\ -\frac{GM}{r}, & \text{otherwise.} \end{cases} \quad (\text{B17})$$

We consider only stars with $E < E_t \equiv -GM/r_t$, which guarantees the stars to be confined inside the truncated radius r_t . Thus, bound orbits within the truncated sphere

are allowed if $-\infty < E < E_t$. In this range of E , there are two real and positive solutions for equation (3), or equivalently,

$$-2(Er_t^2 + GMr_t) \left(\frac{r}{r_t} \right)^2 + 2GMr_t \left(\frac{r}{r_t} \right)^2 \ln\left(\frac{r}{r_t}\right) + L^2 = 0, \quad (\text{B18})$$

if and only if

$$0 < D < \frac{1}{2\exp(1)}, \quad (\text{B19})$$

where

$$D \equiv \frac{L^2}{2GMr_t \exp\left[2\left(1 + \frac{r_t E}{GM}\right)\right]}. \quad (\text{B20})$$

In this allowed region, two real and positive solutions are as follows:

$$r_i = r_t \exp\left(1 + \frac{r_t E}{GM}\right) x_i, \quad (i = \text{apo or peri}; r_{\text{apo}} > r_{\text{peri}}) \quad (\text{B21})$$

with x_{apo} and x_{peri} are the solutions for

$$x^2 \ln x + D = 0. \quad (\text{B22})$$

By this equation, D has a one-to-one correspondence to e , so with x_{peri} and x_{apo} . Use of these quantities gives

$$T_r = \sqrt{\frac{2r_t^3}{GM}} \exp\left(1 + \frac{r_t E}{GM}\right) \int_{x_{\text{peri}}}^{x_{\text{apo}}} \frac{xdx}{\sqrt{-D - x^2 \ln x}}, \quad (\text{B23})$$

$$L^2 = 2GMr_t D \exp\left[2\left(1 + \frac{r_t E}{GM}\right)\right], \quad (\text{B24})$$

and

$$\left(\frac{\partial L^2}{\partial e}\right)_E = -GMr_t \exp\left[2\left(1 + \frac{r_t E}{GM}\right)\right] \\ \times \frac{(x_{\text{apo}} + x_{\text{peri}})^2}{x_{\text{apo}}x_{\text{peri}}} \left[\frac{1}{x_{\text{apo}}^2 - 2D} - \frac{1}{x_{\text{peri}}^2 - 2D} \right]^{-1}. \quad (\text{B25})$$

Consequently, we obtain

$$n_\beta(E, e) = 4\sqrt{2}\pi^2 \sqrt{GMr_t^5 [2GMr_t D]^{-\beta}} \\ \times \exp\left[(3 - 2\beta) \left(1 + \frac{r_t E}{GM}\right)\right] \\ \times \frac{(x_{\text{apo}} + x_{\text{peri}})^2}{x_{\text{apo}}x_{\text{peri}}} \left[\frac{1}{x_{\text{apo}}^2 - 2D} - \frac{1}{x_{\text{peri}}^2 - 2D} \right]^{-1} \\ \times \int_{x_{\text{peri}}}^{x_{\text{apo}}} \frac{xdx}{\sqrt{-D - x^2 \ln x}}. \quad (\text{B26})$$

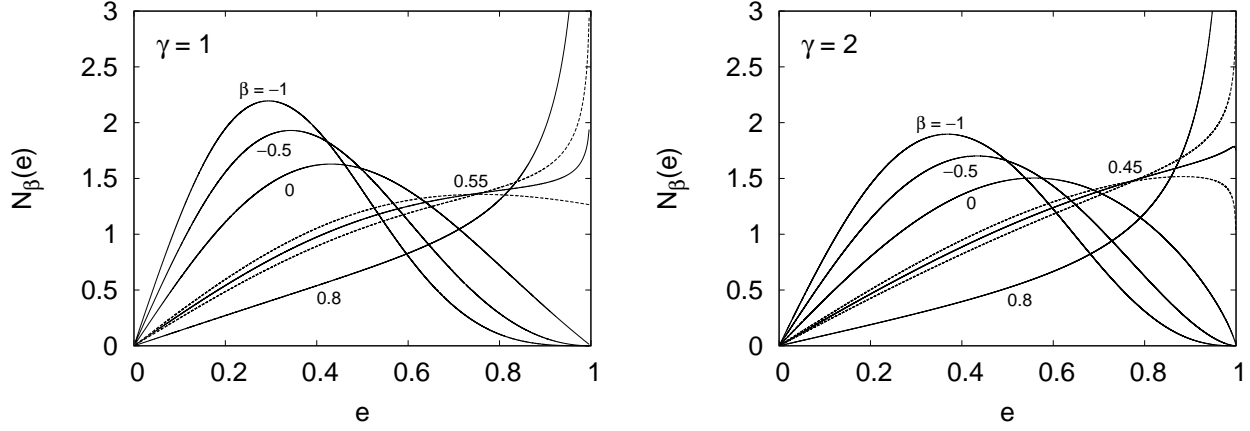


Figure B1. Differential distribution of stellar orbital eccentricity $N_\beta(e)$ in two cases of truncated mass distribution, such as the linear potential model ($\gamma = 1$) on the left panel and the singular isothermal model ($\gamma = 2$) on the right panel. The results are shown by lines for several values of velocity anisotropy parameter β . If $N_\beta(e)$ near $e = 1$ sensitively changes at some particular value of β , the results for $\beta \pm 0.05$ are additionally shown by dotted lines for the purpose of illustrating its sensitivity. Note that $N_\beta(e)$ is normalized such that $\int_0^1 N_\beta(e) + de = 1$.

Since D , x_{peri} , and x_{apo} depend only on e , $n_\beta(E, e)$ is separable in E and e , so that

$$\begin{aligned}
 N_\beta(e) &= 4\sqrt{2}\pi^2 \sqrt{GM r_t^5} [2GM r_t D]^{-\beta} \\
 &\times \left[\int g(E) \exp \left[(3 - 2\beta) \left(1 + \frac{r_t E}{GM} \right) \right] dE \right] \\
 &\times \frac{(x_{\text{apo}} + x_{\text{peri}})^2}{x_{\text{apo}} x_{\text{peri}}} \left[\frac{1}{x_{\text{apo}}^2 - 2D} - \frac{1}{x_{\text{peri}}^2 - 2D} \right]^{-1} \\
 &\quad \times \int_{x_{\text{peri}}}^{x_{\text{apo}}} \frac{x dx}{\sqrt{-D - x^2 \ln x}}. \quad (\text{B27})
 \end{aligned}$$

Thus, the shape of $N_\beta(e)$ is not affected by $g(E)$, like the point mass model and the truncated model with any γ . The results of $N_\beta(e)$ in the singular isothermal model are shown on the right panel of Figure B1. We see that $N_\beta(e)$ shows a monotonically increasing e -distribution for $\beta > 0.45$, while having a single peak for $\beta < 0.45$.